Electronic Supplementary Information

Enhanced electrocatalytic performance for hydrogen evolution reaction through surface enrichment of platinum nanocluster alloying with ruthenium in-situ embedded in carbon

Kui Li,[ab] Yang Li,[abcd] Yuemin Wang,[abc] Junjie Ge,*[ab] Changpeng Liu *[ab] and Wei Xing *[abd]

*Corresponding author: Changpeng Liu, E-mail: liuchp@ciac.ac.cn

Tel.: 86-431-85262225; Fax: 86-431-85262225

* Corresponding author: Junjie Ge, E-mail: gejj@ciac.ac.cn

Tel.: 86-431-85262225; Fax: 86-431-85262225

* Corresponding author: Wei Xing, E-mail: xingwei@ciac.ac.cn

Tel.: 86-431-85262223; Fax: 86-431-85262225

[a] Laboratory of Advanced Power Sources, Changchun Institute of Applied Chemistry, Chinese Academy of Sciences, Changchun, Jilin, 130022, PR China

[b] Jilin Province Key Laboratory of Low Carbon Chemical Power Sources, Changchun, Jilin, 130022, PR China

[c] University of Science and Technology of China, Hefei, Anhui, 230026, PR China

[d] State Key Laboratory of Electroanalytical Chemistry, Changchun Institute of Applied Chemistry, Chinese Academy of Sciences, Changchun, Jilin, 130022, PR China

Experimental section:

1 Synthesis of metal nanoparticles embedded on resorcinol-formaldehyde resin carbon sphere (Ru@RFCS, Pt@RFCS or PtRu@RFCS) catalyst.

The Ru@RFCS, Pt@RFCS or PtRu@RFCS was synthesized by heating mixtures of resorcinol-formaldehyde resin (a carbon precursor) and metal precursor (ruthenium trichloride: $RuCl_3$; chloroplatinic acid: H_2PtCl_6). The preparation process of the support materials was similar with our former works and the preparation method of RFCS could be also obtained from that.[1, 2] We should emphasized that the reaction time is constant (twenty four hours). In a typical process, a mixture containing certain amount of ammonium, as the catalyst, and 400 mg resorcinol were dispersed in 50 mL distilled deionized water, magnetically stirring for 30 min. Then the solution was heated at 94°C while 0.560 mL aqueous formaldehyde solution was added and stirred under reflux, which time is set as the starting time. After t_{add} (t_{add} =2, 6, 12, and 20 hours), we added the metal precursor as the metal source during the reaction. Twenty four hours later, the suspension was vacuum-dried at room temperature and milled to obtain an orange resin powder, and then programmed calcined at 400°C for metal reduction and 900°C for RFCS carbonization in an Ar-H_2 (10%) gas atmosphere. Afterward, the PtRu@RFCS-t_{add}, Pt@RFCS-t_{add} or PtRu@RFCS-t_{add} were obtained after being ground into a powder and washed with deionized water.

2 Synthesis of the PtRu based catalysts deposited on supports materials.

PtRu/RFCS catalysts with a loading of 0.2 wt. % for Pt and 5 wt. % for Ru were synthesized through

impregnation reduction method with sodium borohydride ($NaBH_4$) as the reducing agent. Firstly, 100 mg of RFCS was suspended in 100 ml deionized water and ultrasonically dispersed for 1 h. And 570 μL H_2PtCl_6 solution (3.7 mg $_{Pt}$ mL^{-1}) and 456 μL $RuCl_3$ solution (11.557 mg $_{Ru}$ mL^{-1}) were separately added, after which the mixture was stirred for 30 min to facilitate the impregnation of the metal ions onto the support. Then, a 5 mL $NaBH_4$ solution (2 mg mL^{-1}) was added dropwise under continuous stirring. Subsequently, the suspension was filtered and washed with deionized water and dried at 80°C for 10 h to obtain the as-prepared catalysts.

3 Physical characterizations

Transmission electron microscopy (TEM), high-resolution transmission electron microscopy (HRTEM) and high-angle annular dark-field scanning transmission electron microscopy (STEM) were conducted on a on a Philips TECNAI G2 electron microscope operated at 200 kV. Energy dispersive X-ray analysis (EDX) and element mapping analysis were conducted on a XL30 ESEM FEG field emission scanning electron microscope (SEM) operating at 20 kV. X-Ray photoelectron spectroscopy (XPS) measurements were carried out on a Kratos XSAM-800 spectrometer with an Mg Kα radiation source. X-Ray diffraction (XRD) measurements were performed with a PW1700 diffract meter (Philips Co.) using a Cu Kα (λ=0.15405 nm) radiation source. The obtained XRD patterns were analyzed with Jade 5.0 software to remove the background radiation. The textural and morphological features of the different carbon supports and catalysts prepared were determined by means of nitrogen physisorption at 77 K in a Quantachrome Autosorb-iQ. Textural properties such as specific surface

area, pore volume, and pore size distribution were calculated from each corresponding N_2 adsorption-desorption isotherm applying the Brunauer-Emmet-Teller (BET) equation and Barrett-Joyner-Halenda (BJH) and t-plot methods in ASiQwin 3.01 program. All elemental analyses of catalyst samples were analyzed by ICP-MS (Inductively coupled plasma mass spectrometer) on a Thermo Elemental IRIS Intrepid. Thermo-gravimetric analysis was performed on a thermogravimetric analyzer (TGA Q-50) over a temperature range of 50~900°C at a heating rate of 10°C min^{-1}.

4 Electrochemical measurements

Electrochemical measurements were carried out with an EG & G PARSTAT 4000 potentiostat/galvanostat (Princeton Applied Research Co., USA) in a conventional three electrode test cell. The catalyst ink was prepared by ultrasonically dispersing a mixture containing 5 mg of catalyst, 950 μL of ethanol and 50 μL Nafion solution (Sigma Aldrich, 5 wt. %). Next, 5 μL of the dispersion was pipetted onto a pre-cleaned glassy carbon electrode (GCE, polished with 0.3 and 0.05 mm alumina powder, sonicated and rinsed with deionized water) with 3 mm diameter (area: 0.0707 cm^2; loading 354 μg cm^{-2}) as the working electrode. A graphite rod was used as the counter and the reference electrodes. The saturated calomel electrode (SCE) was applied as reference electrode in acidic. All of the potentials reported in our work were vs. the reversible hydrogen electrode (RHE), unless otherwise noted. For SCE, E (RHE) = E (SCE) + 0.245 V in 0.5 M H_2SO_4. Commercial Pt/C-JM catalysts (20%, Alfa Aesar) was used as a reference to evaluate the electrocatalytic performance of various samples.

The electrolyte (0.5 M H_2SO_4) was degassed by bubbling O_2 for at least 30 minutes prior to electrochemical measurements. Before recording the hydrogen evolution reaction (HER) activity, the catalysts were activated by 10 cyclic voltammetry (CV) scans along the potential window from 0 to -0.6 V vs. SCE in 0.5 M H_2SO_4 at a scan rate of 100 mV s^{-1}, then linear sweep voltammetry (LSV) with a scan rate of 5 mV s^{-1} was performed. During the electrochemical experiments, the electrolyte was agitated using a magnetic stirrer rotating at 300 rpm. To estimate the electrochemical active surface areas (ECSA) of the catalysts, 99.99% pure CO was purged to the cells filled with 0.5 M H_2SO_4 electrolyte for 30 min while the working electrode was held at 0.02 V vs. SCE. N_2 was then purged to the system for 30 min to remove non-adsorbed CO before the measurements were made. The CO stripping was performed in the potential range of -0.2~1.0 V at a scan rate of 50 mV s^{-1}. Assuming that the Coulombic charge required for the oxidation of the CO monolayer was 420 μC cm^{-2}. Accelerated degradation tests (ADTs) were then conducted by CV scanning from 0 to -0.6 V vs. SCE for 5000 cycles at a scan rate of 100 mV s^{-1} to investigate the cycling stability. The durability of the as-prepared catalysts was also investigated through chronopotentiometry (CP), and the timed-pendent voltage was recorded under a static current density of 10 mA cm^{-2} for 48 hours. The electrochemical impedance spectroscopy (EIS) measurements were conducted from 100 kHz to 1 Hz in 0.5 M H_2SO_4. The amplitude of the sinusoidal potential signal was 10 mV. Prior to recording measurements, a resistance test was performed, and *iR* compensation was applied using the EG & G PARSTAT 4000 potentiostat/galvanostat software.

Ohmic drop was corrected using the current interrupt method. All data were corrected for 90% *iR* potential drop (R, ohmic drop 6~8 Ω), unless otherwise noted.

To quantitatively detect the exposed Ru that maybe really participates in electro-catalysis, the filtrates obtained from washing the as-synthesized catalysts with the aqua regia, are measured by ICP-MS. The results indicate that the exposed Ru content is 4.31 wt.% to Ru@RFCS-6h, as well as 1.98, 4.86 and 2.57 wt.% to Ru@RFCS-2h, 12h, 20h, respectively, which is basically in accordance with the trends of the variation in addition time, with only Ru@RFCS-20h as an exception. Additionally, thermo-gravimetric analysis (TGA) is employed to study the total Ru content (including the encapsulated one) in the Ru@RFCS. As shown in **Fig. S1 inset**, the residual weights of the as-prepared catalysts after annealing at high temperature in air atmosphere, are all about 5 wt.% (the concerted value as listed in **Table S1**) approximately approaching to the initial input, except the Ru@RFCS-20h (2.51 wt.%). The reduced in Ru content is ascribed to the following reason: With the condensation reaction proceeding, there are fewer and fewer functional groups to immobilize $[RuCl_5]^{2-}$ complex at the RF surface, which are also not sufficiently reduced by decreasing isolated formaldehyde, as demonstrated by the color changes of product filtrates due to reaction with $NaBH_4$ (**Fig. S2**). **Fig. S1** also shows the as-prepared catalysts with earlier addition time obtain higher decomposition temperature, which may be caused by the enhanced degree of graphitization from metal-catalyzing.

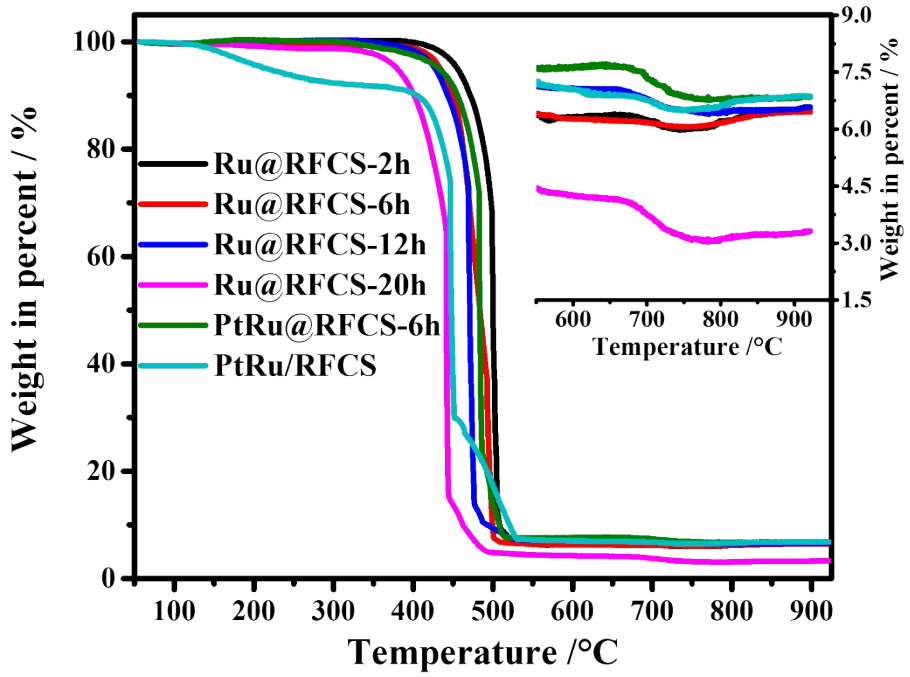

Fig. S1 The TGA curves of Ru@RFCS, PtRu@RFCS-6h and PtRu/RFCS catalysts. The inset shows the final metal oxide content of these catalysts range from 550 to 900ºC with enlarge scale.

Table S1 The mass fraction of metal in all catalysts obtained from TGA curves and ICP-MS measurement.

Catalysts	Calculations from TGA in percent (wt. %)	ICP-MS results[b] (ppm)		Calculations from ICP-MS in percent (wt. %)	
	Pt and Ru	Pt	Ru	Pt	Ru
Ru@RFCS-2h	4.95	-	198	-	1.98
Ru@RFCS-6h	4.93	-	431	-	4.31
Ru@RFCS-12h	4.99	-	486	-	4.86
Ru@RFCS-20h	2.51	-	257	-	2.57
PtRu@RFCS-6h	5.18	16	426	0.16	4.26
PtRu/RFCS	5.21	21	503	0.21	5.03
Pt/C-JM	-	1982	-	19.82	-

[a] The metal weight percent was converted from the final value in TGA based on RuO_2 or PtO_2.

[b] Here, the volume of sample is 10 mL, which was filtrated from washing the as-synthesized catalysts (100 mg) with the aqua regia (10 mL).

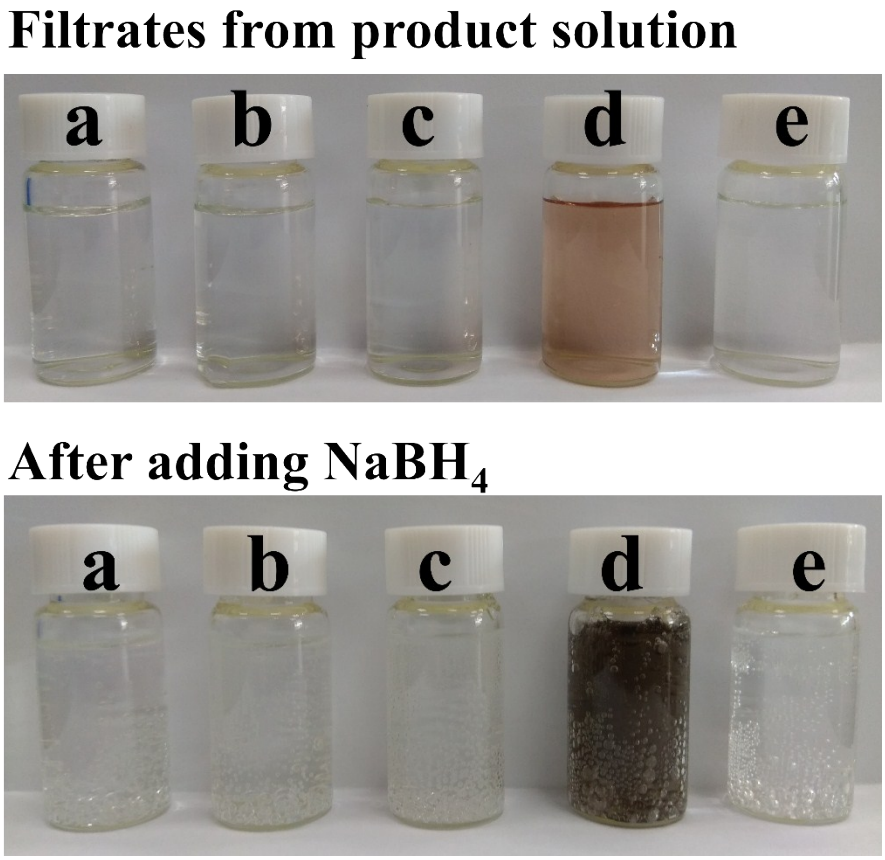

Fig. S2 The upper photo shows the filtrates from the product solution and the below one records color change of the liquid after adding $NaBH_4$. The symbol a, b, c, d and e represent the Ru@RFCS-2h, 6h, 12h, 20h and PtRu@RFCS-6h, respectively.

The as-synthesized partially-embedded catalysts are carefully observed by SEM (**Fig.S3**) to confirm that all metal nanoparticles are uniformly confined in the mesoporous carbon sphere. In **Fig. S3a** for PtRu/RFCS, the isolated carbon spheres ca. 500 nm are observed, with an amount of metal particles located on the external carbon surface (the white points). Considering that the PtRu@RFCS-6h and Ru@RFCS-6h catalysts in **Fig. S3b-c** thermally treated at 900°C for the carbonization of impregnated poly, all the carbon spheres are in monodisperse with a uniform size about 350 nm resulting Ru or PtRu alloy nanoparticles are thus in-situ confined in the nonporous of resorcinol-formaldehyde carbon, rather than situate at the external boundary of the carbon shells.

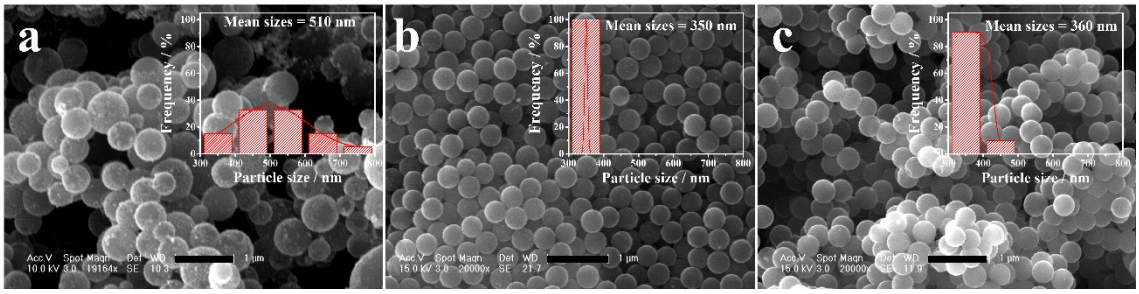

Fig. S3 SEM images of (a) PtRu/RFCS, (b) PtRu@RFCS-6h and (c) Ru@RFCS-6h catalysts; The scale bar is 1 μm.

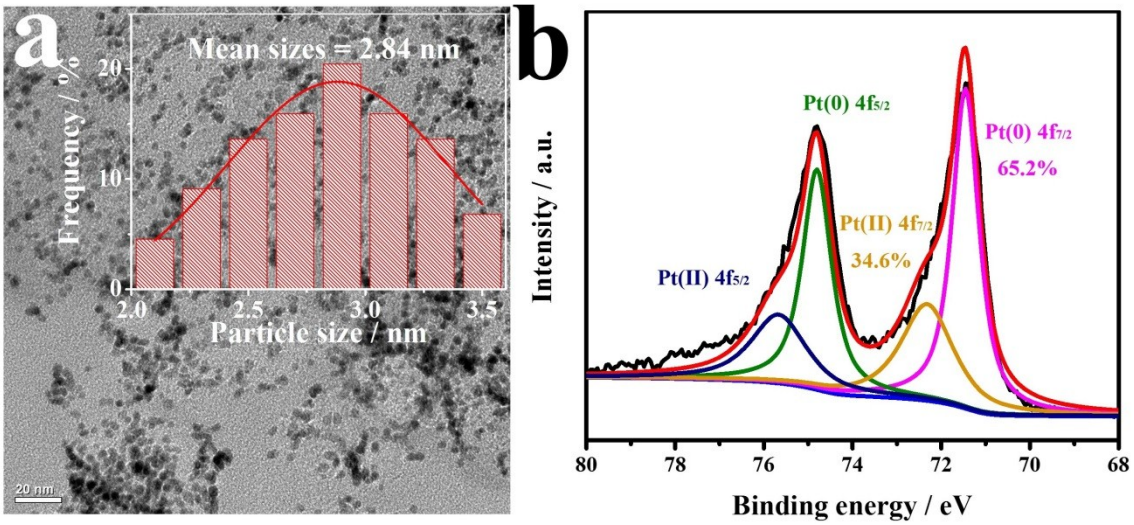

Fig. S4 TEM images and particle sizes distribution histogram (a) and XRD patterns (b) of Pt/C-JM catalyst.

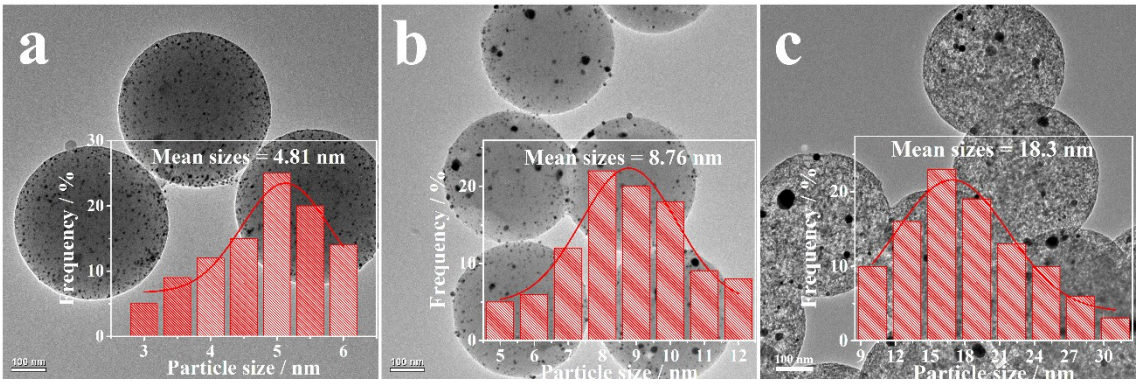

Fig. S5 TEM images and the corresponding particle size distribution histograms of Ru@RFCS catalysts: a, b, and c represents the Ru@RFCS-2h, 12h and 20h, respectively.

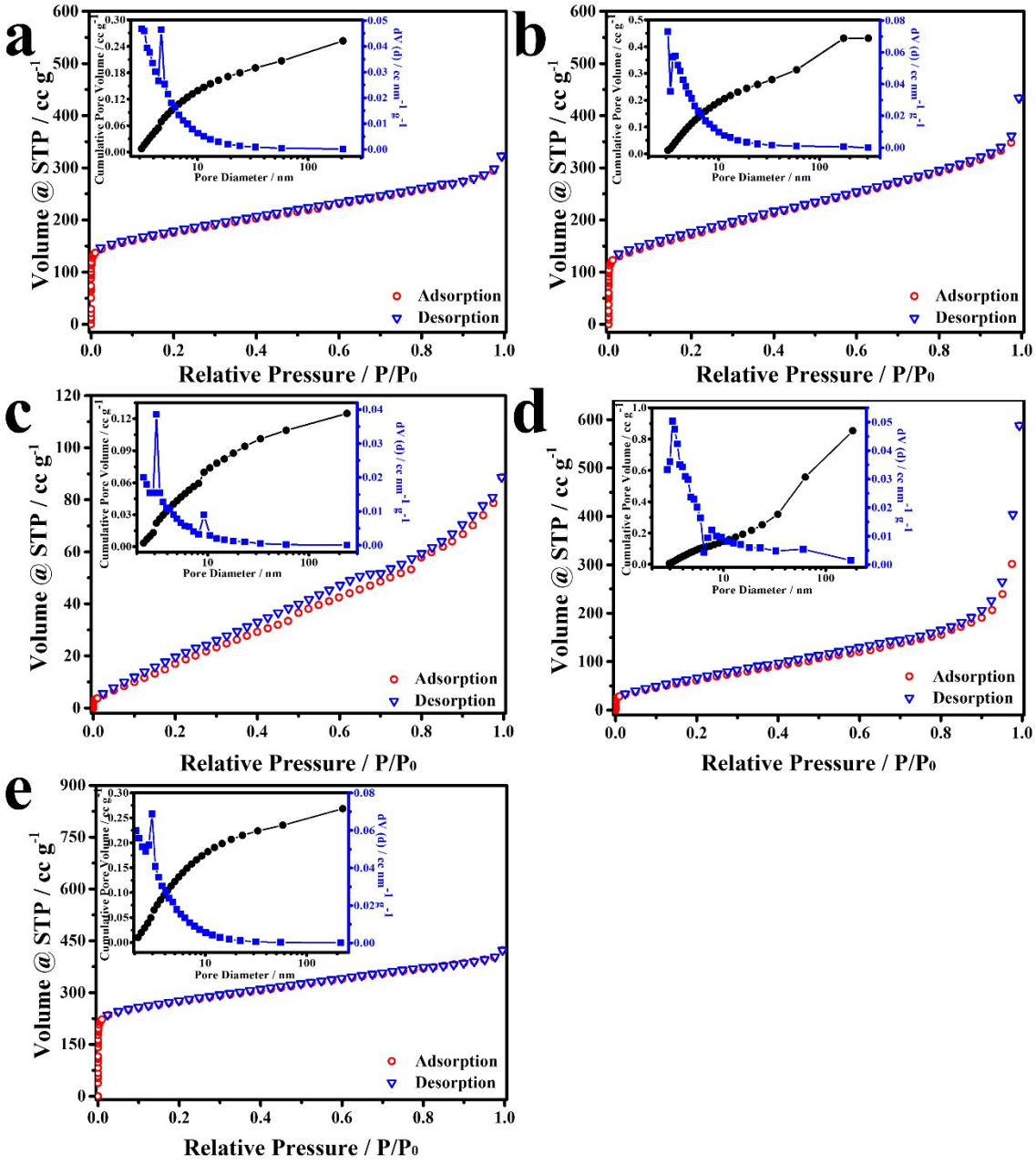

Fig. S6 Typical N_2 adsorption-desorption isotherm and BJH pore size distribution plots (inset) of (a) PtRu@RFCS-6h, (b) Ru@RFCS-6h, (c) PtRu/RFCS (d) Pt/C-JM and (e) Pure RFCS.

Table S2 BET surfaces area (S_{BET}), BJH desorption average pore size and pore volume of PtRu@RFCS-6h, Ru@RFCS-6h, PtRu/RFCS, Pt/C-JM catalysts and pure RFCS.

Catalysts	S_{BET} (m^2 g^{-1})	Average pore size (nm)	Pore Volume (cc g^{-1})
PtRu@RFCS-6h	630.3	3.14	1.397
Ru@RFCS-6h	603.8	3.14	1.405
PtRu/RFCS	105.2	3.13	0.137
Pt/C-JM	259.8	3.32	0.913
Pure RFCS	1016.5	3.12	0.654

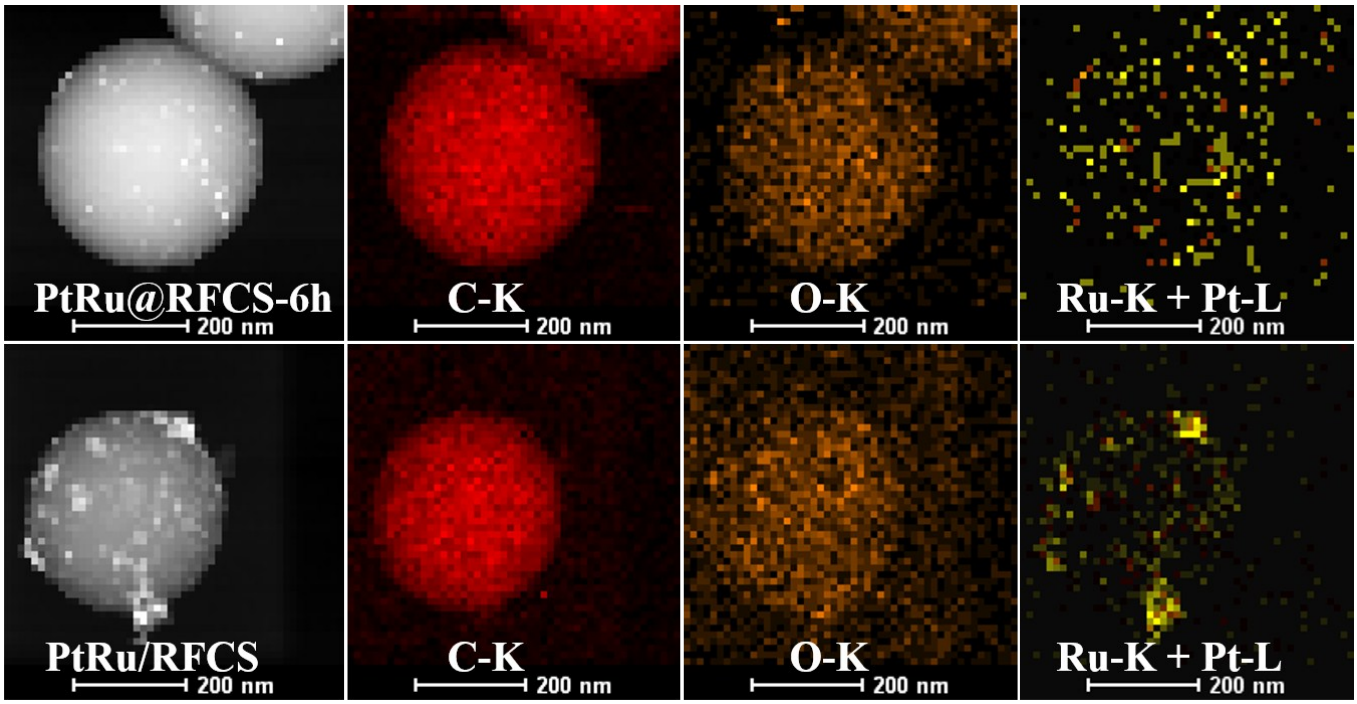

Fig. S7. HAADF-STEM image and the corresponding elemental (Pt, Ru, C, O) mapping images of PtRu@RFCS-6h and PtRu/RFCS catalysts.

Table S3 Particle size of Ru@RFCS, PtRu@RFCS-6h and PtRu/RFCS catalysts obtained by TEM and XRD measurements.

Catalysts	Particles size (nm)	
	By TEM	By XRD
Ru@RFCS-2h	4.81	--
Ru@RFCS-6h	2.65	2.56
Ru@RFCS-12h	8.76	--
Ru@RFCS-20h	18.3	--
PtRu@RFCS-6h	2.57	2.51
PtRu/RFCS	5.12	6.36

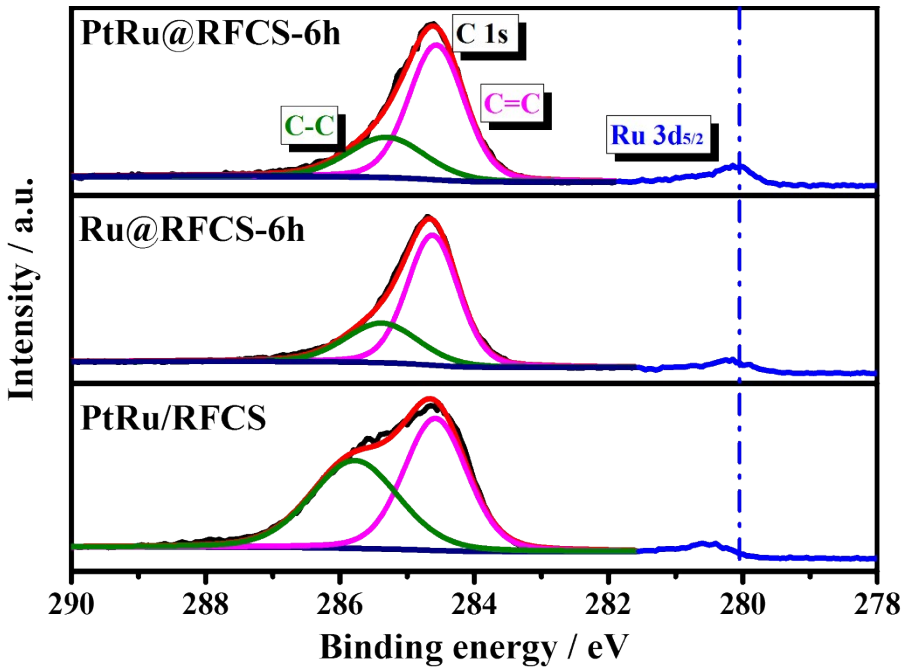

Fig. S8 XPS patterns of PtRu@RFCS-6h, Ru@RFCS-6h and PtRu/RFCS catalysts for C 1s and Ru $3d_{5/2}$ binding energy.

Table S4a Binding energies of the Ru $3p_{5/2}$ and Pt $4f_{7/2}$ components for the PtRu@RFCS-6h, Ru@RFCS-6h and PtRu/RFCS catalysts.

Catalysts	Ru $3p_{5/2}$			Pt $4f_{7/2}$		
	Assignment	Binding energy (eV)	Relative Intensity (%)	Assignment	Binding energy (eV)	Relative Intensity (%)
PtRu@RFCS-6h	Ru(0)	461.53	60.8	Pt(0)	71.58	70.6
	RuO_x	463.74	39.2	Pt(II)	73.17	29.4
PtRu/RFCS	Ru(0)	461.80	47.6	Pt(0)	71.81	46.6
	RuO_x	463.31	52.4	Pt(II)	73.75	53.4
Ru@RFCS-6h	Ru(0)	461.50	58.7	-	-	-
	RuO_x	463.29	41.3	-	-	-

Table S4b Binding energies of the C 1s and Ru $3d_{5/2}$ components as well as O/C ratio for the PtRu@RFCS-6h, Ru@RFCS-6h and PtRu/RFCS catalysts.

Catalysts	C 1s			Ru $3d_{5/2}$	O/C ratio (%)
	Assignment	Binding energy (eV)	Relative Intensity (%)	Binding energy (eV)	
PtRu@RFCS-6h	C=C	284.56	70.7	280.05	1.54
	C-C	285.31	29.3		
PtRu/RFCS	C=C	284.58	52.2	280.51	6.41
	C-C	285.78	47.8		
Ru@RFCS-6h	C=C	284.62	69.7	280.17	1.39
	C-C	285.38	30.3		

To determine the optimized one at time-dependence for Ru@RFCS, it is shown in **Fig. S9** (LSV polarization curves, *iR* compensated) that the as-prepared electrocatalysts possess the different onset overpotential range from 17.4 mV to 76.3 mV as listed in **Table S5**. And to obtain the 10 mA cm^{-2} HER current density, the Ru@RFCS-6h catalyst requires the lowest overpotential of 58.1 mV among those as-regulated catalysts, indicating the highest catalytic activity. These results reveal that controlling the addition time at 6 hours maybe expose the most abundant active site for Ru@RFCS in HER.

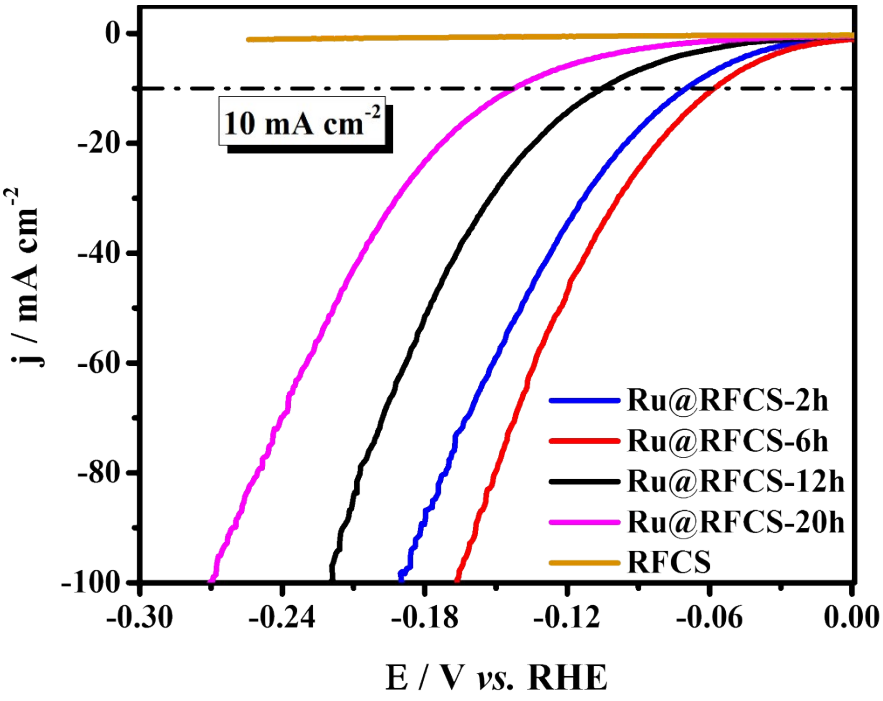

Fig. S9 Polarization curves of all Ru@RFCS catalysts in 0.5 M H_2SO_4. The catalyst loading was 350 μg cm^{-2} and the electrode area was 0.0707 cm^2.

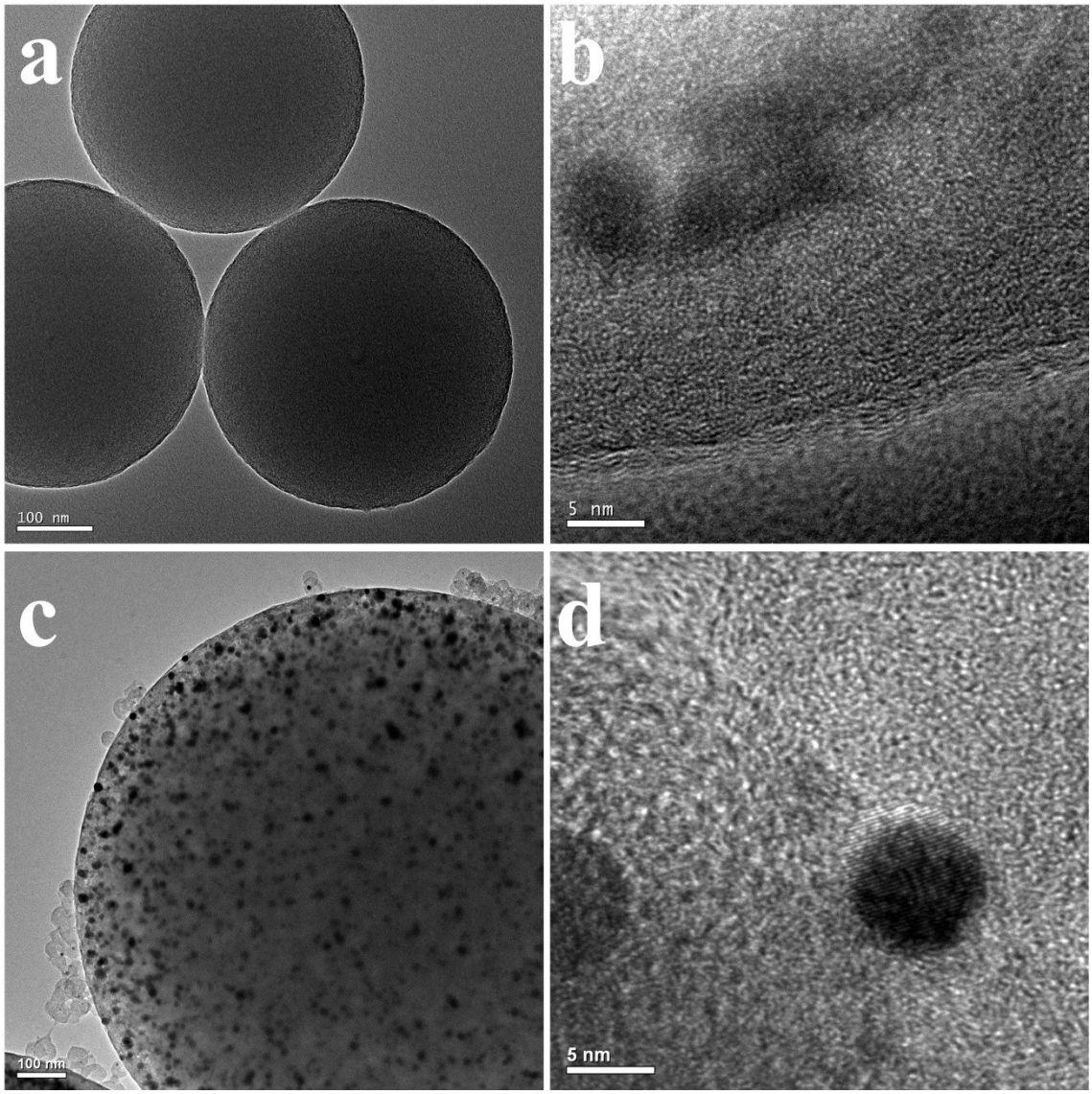

Fig. S10 TEM and HRTEM images of Pt@RFCS catalysts: (a, b) represent the Pt@RFCS-6h-0.2%; (c, d) represent the Pt@RFCS-6h-20%.

Table S5 The comparison of overpotential (η) at different current density (*iR* compensated), turnover Frequency (TOF) and hydrogen production in cost at a η of 100 mV for PtRu@RFCS-6h, Pt@RFCS, all Ru@RFCS, PtRu/RFCS and Pt/C-JM catalysts in 0.5 M H_2SO_4.

Catalysts	η (mV)			TOF @ η=100 mV (H_2 s^{-1} per active site)[b]	hydrogen production in cost @ η=100 mV (L_{H2} s^{-1} per dollar)[c]
	Onset[a]	@10 mA cm^{-2}	@100 mA cm^{-2}		
PtRu@RFCS-6h	2.3	19.7	43.1	4.03	1.53
Pt@RFCS-6h-0.2%	303.3	385	-	-	-
Pt@RFCS-6h-20%	5.1	21.6	45.3	-	-
Ru@RFCS-2h	27.3	70.1	189.5	-	-
Ru@RFCS-6h	17.4	58.1	166.4	0.215	0.147
Ru@RFCS-12h	49.1	105.2	220.6	-	-
Ru@RFCS-20h	76.3	142.5	270.7	-	-
PtRu/RFCS	15.8	46.6	145.3	0.375	0.106
Pt/C-JM	0	19.5	61.8	1.25	0.012

[a] The onset overpotential (η) was achieved at 2 mA cm^{-2} in LSV.

[b] TOF was calculated using the following formula:

$$TOF = \left(j\frac{mA}{cm^2}\right)\left(\frac{1\ C\ s^{-1}}{1000\ mA}\right)\left(\frac{1\ mol\ e^{-1}}{96485\ C}\right)\left(\frac{1\ mol\ H_2}{2\ mol\ e^{-1}}\right)\left(\frac{6.02\times10^{23}\ H_2\ molecules}{1\ mol\ H_2}\right)$$

$$= 3.12\times10^{15}\frac{H_2\ s^{-1}}{cm^2}\ per\ \frac{mA}{cm^2} \qquad \textbf{Equation 1}$$

The number of active sites per real surface area for Ru@RFCS and Pt/C-JM are obtained from the unit cell of Ru and Pt:

$$\#\ active\ sites\ Ru = \left(\frac{2\ atoms/unitcell}{2.702\ nm^3/unitcell}\right)^{2/3} = 1.76 \times 10^{15}\ atoms\ cm^{-2}$$ **Equation 2**

$$\#\ active\ sites\ Pt = \left(\frac{4\ atoms/unitcell}{6.038\ nm^3/unitcell}\right)^{2/3} = 1.64 \times 10^{15}\ atoms\ cm^{-2}$$ **Equation 3**

Therefore, the TOF value can be obtained from the following formula:

$$TOF = \frac{\left(3.12 \times 10^{15} \frac{H_2\ s^{-1}}{cm^2}\ per\ \frac{mA}{cm^2}\right) \times |j|}{\#\ active\ sites \times A_{ECSA}}$$ **Equation 4**

[c] Hydrogen production in cost (HPC) was calculated using the following procedures:

Firstly, the prices per electrode area (0.707 cm^{-2}) of the four comparison catalysts

$$Price_{sample}\ per\ cm^2 = catalyst\ load \times (\$988\ oz \times Pt\ wt.\% + \$42\ oz \times Ru\ wt.\%)$$ **Equation 5**

The catalyst load per cm^2 was 354 μg. And according to **Equation 1**,

$$HPC_{sample} = 3.12 \times 10^{15} \frac{H_2\ s^{-1}}{Price_{sample} \times N_A \times V_m}\ per\ \frac{mA}{cm^2} = \frac{4.17932 \times 10^{-4}}{Price_{sample}}\ L\ h^{-1}\ per\ j$$ **Equation 6**

For example, the HPC of PtRu@RFCS-6h in 0.5 M H_2SO_4 is calculated as

$$Price_{PtRu@RFCS-6h}\ per\ cm^2 = 354\ \mu g \times (\$988\ per\ oz \times 0.2\ wt.\% + \$42\ per\ oz \times 5\ wt.\%) = \$4.96 \times 10^{-5}\ per\ cm^2$$

$$HPC_{PtRu@RFCS-6h} = 3.12 \times 10^{15} \frac{H_2\ s^{-1}}{\$4.96 \times 10^{-5}} \frac{1}{N_A \times V_m}\ per\ j = 8.424\ L\ h^{-1}\ per\ dollar\ per\ j$$

Electrochemical capacitance was measured by cyclic voltammograms at different scan rates of 20, 40, 60, 80, 120, 160, 240 and 320 mV s^{-1} (Fig. S11). The capacitive currents were collected where no apparent Faradic processes were observed. These measured capacitive currents were then plotted as a function of scan rates in Fig. S11e. Linear fitting revealed that the specific capacitance was 12.25, 10.31, 8.84 and 11.47 mF cm^{-2} for PtRu@RFCS-6h, Ru@RFCS-6h, PtRu/RFCS and Pt/C-JM catalysts in 0.5 M H_2SO_4. Assuming that the specific capacitance of a flat surface is ~ 40 μF for 1 cm^2 of real surface area, then the ECSA is estimated as:

$$A_{ECSA}^{sample} = \frac{specific\ capacitance}{40\ \mu F\ cm^{-2}\ per\ cm_{ECSA}^{2}}$$

Equation 7

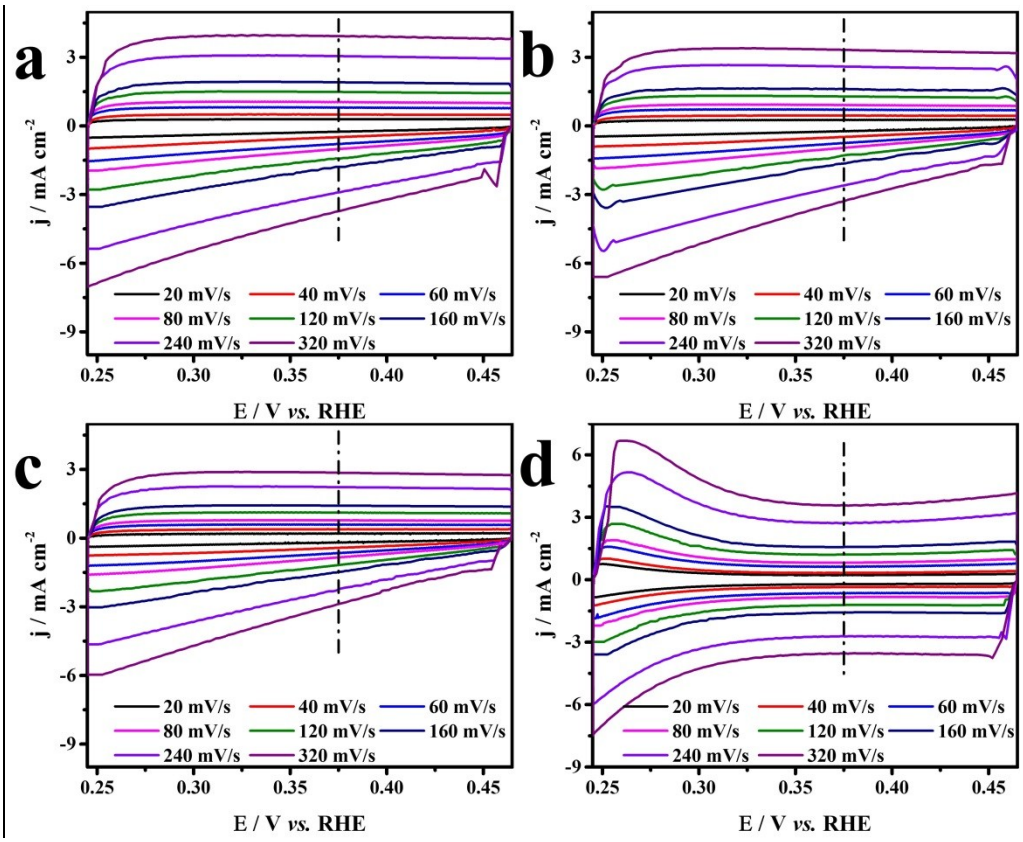

Fig. S11 CVs of PtRu@RFCS-6h (a), Ru@RFCS-6h (b), PtRu/RFCS (c) and commercial Pt/C-JM (d) catalysts with different scan rates in 0.5 M H_2SO_4 solution. The capacitive currents were collected at 0.375 V *vs.* RHE in potential range where no Faradaic processes were present.

Table S6 Summary of some recently reported representative precious metal hybrid catalysts for HER in acidic electrolytes (0.5 M H_2SO_4).

Catalyst	Precious metal loading amount	Current density (*j*, mA cm^{-2})	*η@j* (mV)	Tafel Slope (mV dec^{-1})	Reference
PtRu@RFCS-6h	17.7 μg $_{Ru}$ cm^{-2}	10	19.7	27.2	This work
	0.71 μg $_{Pt}$ cm^{-2}	100	43.1		
Ru@RFCS-6h	17.7 μg $_{Ru}$ cm^{-2}	10	58.1	60.5	This work
		100	166.4		
PtCoFe@CN	13.1 μg $_{Pt}$ cm^{-2}	10	45	32	*ACS Appl. Mat. Interfaces 2017, 9, 3596.*[3]
$Pt_{13}Cu_{73}Ni_4$/CNF@CF*	31.1 wt. % (Pt)	5	70	38	*ACS Appl. Mat. Interfaces 2016, 8, 3464.*[4]
$Pt_{81}Fe_{28}Co_{10}$	44.9 μg $_{Pt}$ cm^{-2}	1325	400	21	*Adv Mater. 2016, 28, 2077.*[5]
$Pt_{23}Ni_{77}$/C	5.3 μg $_{Pt}$ cm^{-2}	5.3	287	--	*J. Phys. Chem. C 2015, 119.*[6]
Ru@C_2N	81.8 μg $_{Ru}$ cm^{-2}	10	22	30	*Nat. Nanotechnol.. 2017, 12, 441.*[7]
		20	34.8		
$Ni_{43}Ru_{57}$ nanoalloy	167.8 μg $_{Ru}$ cm^{-2}	10	41	31	*ACS Appl. Mat. Interfaces 2017, 9, 17326.*[8]
Pt ML/Ag NF/Ni foam	0.55 μg $_{Pt}$ cm^{-2}	10	70	53	*Sci. Adv. 2015, 1, e1400268.*[9]
Ru nanosheet	101.8 μg $_{Pt}$ cm^{-2}	1.02	20	46	*ACS Catalysis. 2016, 6, 1487.*[10]
Ru/NG-750	24.2 μg $_{Ru}$ cm^{-2}	10	53	44	*ACS Appl. Mat. Interfaces 2017, 9, 3785.*[11]
$Co_{80}Ru_{15}Pt_5$	2.7 wt. % (Pt) 4.2 wt. % (Ru)	4	73.1	30.4	*Int. J. Hydrogen. Energ. 2017, 42, 38.*[12]
Ru/GLC	40 μg $_{Ru}$ cm^{-2}	10	35	46	*ACS Appl. Mat. Interfaces 2016, 8, 35132.*[13]
		20	61		
		50	125		
Rh_2S_3_ThickHNP/C	13.6 μg $_{Rh}$ cm^{-2}	10	122	44	*Energy Environ. Sci. . 2016, 9, 850.* [14]
	13.6 μg $_{Rh}$ cm^{-2} (After 10000CVs)		97	55	
	81.4 μg $_{Rh}$ cm^{-2}		88	69	
RuP_2@NPC	230.7 μg $_{Ru}$ cm^{-2}	10	38	38	*Angewandte Chemie 2017, 129.*[15]
$Cu_{2-x}S$@Ru NPs	7.7 μg $_{Ru}$ cm^{-2}	10	129	51	*Small 2017, 13, 1700052.* [16]
Ru-MoO_2	84.4 μg $_{Ru}$ cm^{-2}	10	55	44	*J. Mater. Chem. A. 2017, 5,*

					5475[17]
Pd@PdPt	444.2 μg $_{Pd}$ cm^{-2} 121.7 μg $_{Pt}$ cm^{-2}	10	39	38	*J. Mater. Chem. A. 2016, 4, 16690.*[18]
1D-RuO_2-CN_x	170	10	93	40	*ACS Appl. Mat. Interfaces 2016, 8, 28678.*[19]
NiAu/Au	203.7	10	50	36	*J Am Chem Soc. 2015, 137, 5859.*[20]
PdCu@Pd NCs	140	10	65	35	*ACS Appl. Mat. Interfaces 2017, 9, 8151.*[21]
Pt NC/N-graphene-2	5.6 μg $_{Pt}$ cm^{-2}	10	24	28	*Nanoscale. 2017, 9, 10138.*[22]
Rh-Mo_2S	17.0 μg $_{Rh}$ cm^{-2}	10	47	24	*Adv Funct Mater. 2017, 27.*[23]
Pt-Cu/CNFs-1:2	--	10 104	71 300	68	*Advanced Materials Interfaces. 2017, 4.*[24]
Pd-Mn_3O_4-1	18.8μg $_{Pd}$ cm^{-2}	10	14	42	*Chem Commun. 2016, 52, 6095.*[25]
Pt NCs@CIAC-121	--	10 20	48 60	58	*J Am Chem Soc. 2016, 138, 16236.*[26]

* The acidic electrolyte is 1.0 M H_2SO_4.

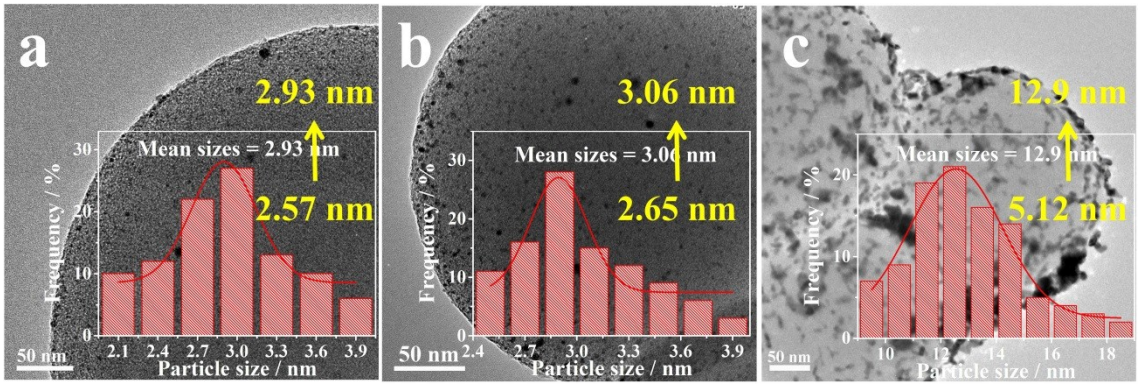

Fig. S12 TEM images and the corresponding particle size distribution histograms of the as-prepared catalysts after ADTs: a, b, and c represents the PtRu@RFCS-6h, Ru@RFCS-6h and PtRu/RFCS, respectively.

References

1. K. Li, J. B. Zhu, M. L. Xiao, X. Zhao, S. K. Yao, C. P. Liu and W. Xing, *ChemCatChem*, 2014, **6**, 3387-3395.
2. K. Li, Z. Jin, J. Ge, C. Liu and W. Xing, *J. Mater. Chem. A*, 2017, **5**, 19857-19865.
3. J. Chen, Y. Yang, J. Su, P. Jiang, G. Xia and Q. Chen, *ACS Appl. Mat. Interfaces* 2017, **9**, 3596-3601.
4. Y. Shen, A. C. Lua, J. Xi and X. Qiu, *ACS Appl. Mat. Interfaces* 2016, **8**, 3464-3472.
5. N. Du, C. Wang, X. Wang, Y. Lin, J. Jiang and Y. Xiong, *Adv Mater*, 2016, **28**, 2077-2084.
6. S. Wang, G. Yang and S. Yang, *J. Phys. Chem. C* 2015, **119**, 27938-27945.
7. J. Mahmood, F. Li, S.-M. Jung, M. S. Okyay, I. Ahmad, S.-J. Kim, N. Park, H. Y. Jeong and J.-B. Baek, *Nat. Nanotechnol.* , 2017, **12**, 441-446.
8. C. Zhang, Y. Liu, Y. Chang, Y. Lu, S. Zhao, D. Xu, Z. Dai, M. Han and J. Bao, *ACS Appl. Mat. Interfaces* 2017, **9**, 17326-17336.
9. M. Li, Q. Ma, W. Zi, X. Liu, X. Zhu and S. Liu, *Sci. Adv.*, 2015, **1**, e1400268-e1400268.
10. X. Kong, K. Xu, C. Zhang, J. Dai, S. Norooz Oliaee, L. Li, X. Zeng, C. Wu and Z. Peng, *ACS Catal.*, 2016, **6**, 1487-1492.
11. R. Ye, Y. Liu, Z. Peng, T. Wang, A. S. Jalilov, B. I. Yakobson, S.-H. Wei and J. M. Tour, *ACS Appl. Mat. Interfaces* 2017, **9**, 3785-3791.
12. J. V. Medina-Flores, A. Manzo-Robledo, J. M. Mora-Hernandez and E. M. A. Estrada, *Int. J. Hydrogen. Energ.*, 2017, **42**, 38-45.
13. Z. Chen, J. Lu, Y. Ai, Y. Ji, T. Adschiri and L. Wan, *ACS Appl. Mat. Interfaces* 2016, **8**, 35132-35137.
14. D. Yoon, B. Seo, J. Lee, K. S. Nam, B. Kim, S. Park, H. Baik, S. H. Joo and K. Lee, *Energy Environ. Sci.* , 2016, **9**, 850-856.
15. Z. Pu, I. S. Amiinu, Z. Kou, W. Li and S. Mu, *Angew Chem Int Edit*, 2017, **56**, 11559-11564.
16. D. Yoon, J. Lee, B. Seo, B. Kim, H. Baik, S. H. Joo and K. Lee, *Small* 2017, **13**, 1700052 1-8.
17. P. Jiang, Y. Yang, R. Shi, G. Xia, J. Chen, J. Su and Q. Chen, *J. Mater. Chem. A*, 2017, **5**, 5475-5485.
18. Y. Liu, S. Liu, Z. Che, S. Zhao, X. Sheng, M. Han and J. Bao, *J. Mater. Chem. A*, 2016, **4**, 16690-16697.
19. T. Bhowmik, M. K. Kundu and S. Barman, *ACS Appl. Mat. Interfaces* 2016, **8**, 28678-28688.
20. H. Lv, Z. Xi, Z. Chen, S. Guo, Y. Yu, W. Zhu, Q. Li, X. Zhang, M. Pan, G. Lu, S. Mu and S. Sun, *J Am Chem Soc*, 2015, **137**, 5859-5862.
21. J. Li, F. Li, S.-X. Guo, J. Zhang and J. Ma, *ACS Appl. Mat. Interfaces* 2017, **9**, 8151-8160.
22. B. Jiang, F. Liao, Y. Sun, Y. Cheng and M. Shao, *Nanoscale*, 2017, **9**, 10138-10144.
23. Y. Cheng, S. Lu, F. Liao, L. Liu, Y. Li and M. Shao, *Adv Funct Mater*, 2017, **27**, 1700359 1-6.
24. J. Wang, J. W. Chen, J. D. Chen, H. Zhu, M. Zhang and M. L. Du, *Adv. Mater. Interfaces*, 2017, **4**, 1700005 1-8.
25. C. Ray, S. Dutta, Y. Negishi and T. Pal, *Chem Commun*, 2016, **52**, 6095-6098.
26. S. Wang, X. Gao, X. Hang, X. Zhu, H. Han, W. Liao and W. Chen, *J Am Chem Soc*, 2016, **138**, 16236-16239.